The Limit of the Total Scattering Cross Section of Electrically Large Stirrers in a Reverberation Chamber

Qian Xu, Yi Huang, *Senior Member, IEEE*, Lei Xing, Zhihao Tian, *Student Member, IEEE*, Chaoyun Song and Manoj Stanley

***Abstract*—The total scattering cross section (TSCS) has been proven to be an effective quantity to characterize the performance of stirrers in a reverberation chamber (RC). It is shown in this letter that the maximum TSCS is a quarter of the stirring surface area, and it is equal to the absorption cross section (ACS) of the same area with perfect radio absorbers. The mathematical proof is presented and measurements are performed to validate this limit. It is also shown that the TSCS and ACS are statistical dual quantities; related dual quantities are also given. The TSCS can be used to characterize how well a stirrer is designed or how close an RC is to a perfect RC.**

***Index Terms*—scattering cross section, reverberation chamber, RC stirrer, RC characterization.**

I. Introduction

THE total scattering cross section (TSCS) has been studied and measured in a reverberation chamber (RC) [1-3]. It has been found that the TSCS is an important parameter used to characterize the ability of an object to scatter the diffuse field, thus it can be used to characterize stirrer performance in an RC and provide guidelines for stirrer design [3]. This is an area which has not attracted a lot of research attention.

In this letter, we will show that there is a limit of the TSCS for a given stirring surface area. The TSCS of stirrers is limited by the stirring surface area. An optimized stirrer structure can only approach this limit but cannot exceed it. It is found in this letter that there exist dual statistical quantities in the RC. For electrically large object, since the limit of absorption cross section (ACS) is already known [4], and the TSCS and ACS are dual quantities. We will show that the limit of TSCS is a quarter of the stirring surface area. By comparing the measured TSCS with this limit one can characterize how well the stirrer is designed. It can be seen that an RC and an anechoic chamber (AC) are also dual environments for averaged *S*-parameters, which means the TSCS could also be used to characterize the performance of an RC.

Manuscript received Oct. 14, 2015. Corresponding author: Y. Huang.

Q. Xu, Y. Huang, L. Xing, Z. Tian, C. Song and M. Stanley are with the Department of Electrical Engineering and Electronics, The University of Liverpool, Liverpool, L69 3GJ, UK (e-mail: qian.xu@liv.ac.uk; yi.huang@liv.ac.uk; l.xing@liv.ac.uk; zhihao.tian@liv.ac.uk; sgcsong2@liv.ac.uk; manoj.stanley@liv.ac.uk).

The letter is organized in four sections. In Section II, the mathematical derivation is given and the dual quantities are obtained. In Section III, measurements are performed to validate the limit. Finally discussions and conclusions are given in Section IV.

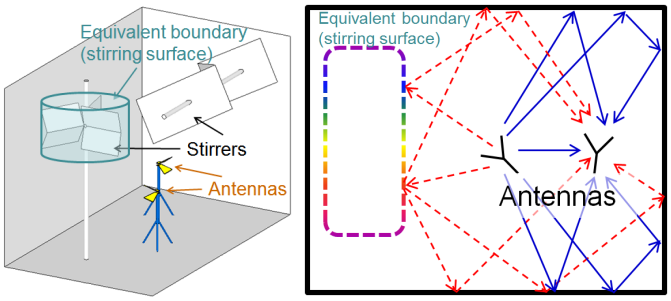

Fig. 1. (a) Measurement scenario and the equivalent boundary (stirring surface), (b) equivalent boundary and all interaction paths between two antennas, the dashed lines represent the stirrer path and the solid lines represent the unstirred part.

II. Theory

We first introduce an equivalent boundary from the full wave point of view and then use a ray model (multipath model [5, 6]) to complete the analysis. A typical measurement scenario is shown in Fig. 1(a). Suppose the vertical stirrer is rotating, then there is an equivalent boundary (stirring surface) which covers the stirrer when it is rotating. When the stirrer is rotated, from the full wave point of view, we just change the boundary condition of each small piece on the equivalent surface. Different boundary condition configurations correspond to different stirrer positions. It should be noted that the equivalent boundary can be chosen arbitrarily as long as it covers the rotating stirrer, but the limit can be considered as the *smallest surface that covers the stirrer when it is rotating*. As can be seen later, when the stirrer is close to the corner (wall) of the RC, the equivalent boundary shown in Fig. 1(a) may not be the smallest surface, the effect of the wall needs to be considered.

Two scenarios are analyzed: an RC with stirring boundary and an RC with absorbing boundary. It can be seen that, interestingly, these two scenarios are dual.

A. RC with Stirring Boundary

The frequency response of the transmission coefficient (S_{21}) can be considered as a superposition of all scattering and reflection paths between two antennas in the RC, as shown in Fig. 1(b). The dashed lines represent the paths that interact with the stirrer (stirred part) while the solid lines represent the paths that do not interact with the stirrer (unstirred part).

Mathematically, the frequency response at each frequency can be expressed as

$$S_{21} = \sum_i H_i(j\omega)E_i = \sum_s H_s(j\omega)E_s + \sum_u H_u(j\omega)E_u \ , \quad (1)$$

where $H_s(j\omega)$ and $H_u(j\omega)$ represent the transfer functions of each stirred path and unstirred path between the transmitting (Tx) and receiving (Rx) antenna respectively, and E_s and E_u are the excitation amplitudes of each path determined by the radiation power and pattern of the transmitting antenna. The reason why $H_s(j\omega)$ and $H_u(j\omega)$ are introduced is that, when averaging the stirred part will cancel each other and only the unstirred part will be left. To simplify the derivation, we can consider the stirrer as a lossless reflector, and the magnitude of the transfer function of each path does not change (as can be seen later, these assumptions are not necessary), and the rotation of the stirrer becomes the stirring of the phase of each path. Thus for each stirrer position (boundary configuration) and each frequency, we have

$$\begin{aligned} S_{21,1} &= \sum_s H_s(j\omega)e^{j\varphi_{s,1}}E_s + \sum_u H_u(j\omega)E_u \ , \\ S_{21,2} &= \sum_s H_s(j\omega)e^{j\varphi_{s,2}}E_s + \sum_u H_u(j\omega)E_u \ , \\ &\vdots \\ S_{21,n} &= \sum_s H_s(j\omega)e^{j\varphi_{s,n}}E_s + \sum_u H_u(j\omega)E_u \ , \end{aligned} \quad (2)$$

where n represents each stirrer position. The averaged S_{21} with N boundary configurations can be obtained as

$$\langle S_{21}\rangle_N = \sum_s \left(H_s(j\omega)E_s \frac{1}{N}\sum_{n=1}^{N} e^{j\varphi_{s,n}}\right) + \sum_u H_u(j\omega)E_u \ . \quad (3)$$

For a well stirred RC, the reflected phases are random, and the distribution of the phase $\varphi_{s,n}$ should be uniform, thus we have

$$\lim_{N\to\infty} \frac{1}{N}\sum_{n=1}^{N} e^{j\varphi_{s,n}} = 0 \ . \quad (4)$$

Equation (3) becomes

$$\lim_{N\to\infty} \langle S_{21}\rangle_N = \sum_u H_u(j\omega)E_u \ , \quad (5)$$

which is the from the unstirred part.

B. RC with Absorbing Boundary

If we replace the equivalent boundary by a perfect absorber/perfect matched layer (PML) as shown in Fig. 2, all the signals that interacting with the PML will be totally absorbed, and (1) becomes

$$S_{21} = \sum_u H_u(j\omega)E_u \ . \quad (6)$$

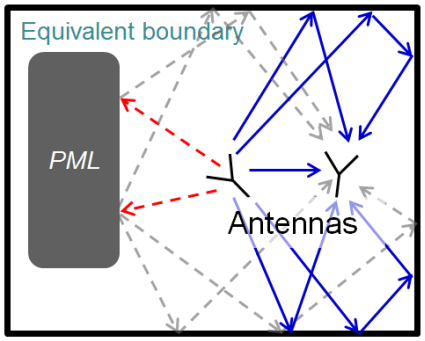

Fig. 2. The equivalent surface is replaced by a PML, waves with light dashed lines are perfectly absorbed.

As can be seen, (5) and (6) are the same. Although in [1], the measurement was performed directly in the time domain, we measured it in the frequency domain and obtain the impulse response by using the inverse fast Fourier transform (IFFT) [7, 8]. In the time domain the decay of $[IFFT\langle S_{21}\rangle]^2$ follows $e^{-t(1/\tau_{RC}+1/\tau_s)}$ [1], where τ_{RC} is the chamber decay time and τ_s is the scattering damping time. By correcting the loss of the RC (including the loss of the stirrer), the scattering damping time can be obtained from the decay speed of $C(t)$, which is defined as [1-3]

$$C(t) = [IFFT\langle S_{21}\rangle]^2 / \langle [IFFT(S_{21})]^2\rangle = e^{-t/\tau_s} \ . \quad (7)$$

Here $\langle\cdot\rangle$ means averaging over all stirrer positions (boundary configurations). Since the chamber loss is corrected in (7), we can consider the walls of the RC in Fig. 1(b) and Fig. 2 as being lossless, thus the decay speed of $[IFFT\langle S_{21}\rangle]^2$ in (7) determines τ_s in Fig. 1(b) and the decay speed of $[IFFT(S_{21})]^2$ in (6) determines τ_{RC} in Fig. 2. Since (5) and (6) are the same, τ_s in the scenario of Fig. 1(b) equals τ_{RC} in the scenario of Fig. 2.

It has been proven that, for an electrically large perfect absorber, the maximum absorption cross section (ACS) is a quarter of the overall surface area of the object and independent of the shape of the object [4], and $ACS = V/(c_0\tau_{RC})$ (all the loss is from the absorber [9]) in Fig. 2, where V is the volume of the RC and c_0 is the speed of light. Based on this, remember $TSCS = V/(c_0\tau_s)$ in Fig. 1(b) [1], thus the theoretical limit of the TSCS of an electrically large *perfect* diffuse wave scatterer is a quarter of the stirring surface area. A summary of dual quantities is given in Table I.

TABLE I
SUMMARY OF DUAL QUANTITIES

In the scenario of Fig. 1(b)		In the scenario of Fig. 2
$\lim_{N\to\infty}\langle S_{21}\rangle_N$	=	S_{21}
τ_s	=	τ_{RC}
$TSCS = \frac{A_s}{4}$	=	$ACS = \frac{A_s}{4}$

A_s represents the stirring surface area in Fig. 1(b) and the PML surface area in Fig. 2, respectively.

It should be noted that, when the RC is heavily loaded (the absorber occupies a large volume in the RC), the power profile of the impulse response no longer decays exponentially (actually no profile, the response is close to the free space response), in this case τ_{RC} and τ_s need to be extracted in a larger RC.

We have assumed the magnitude in each path is invariant when deriving (5). It can be proven that this assumption is unnecessary. Mathematically, an arbitrary complex number H can be expressed by using a superposition of M unit vectors with phases φ_m ($\sum_{m=1}^{M} e^{j\varphi_m}$), where M can be arbitrarily large. In this case, (4) becomes

$$\lim_{N\to\infty} \frac{1}{N} \sum_{n=1}^{N} \sum_{m=1}^{M} e^{j\varphi_{m,s,n}} e^{j\varphi_{s,n}} = 0 . \qquad (8)$$

The distribution of $\varphi_{m,s,n}$ and $\varphi_{s,n}$ are uniform. Thus, the stirring of magnitude can still be regarded as a superposition of phase stirs and the form of (5) still holds valid. The loss of the stirrer can be shifted to the loss of the walls in the RC [5] which was corrected in (7).

III. Measurements

Since $A_s/4$ is the TSCS of a perfect diffuse field scatterer, we can only observe a measured TSCS value lower than $A_s/4$. It is impractical to measure all possible stirrer designs to verify this assumption. In this section, we present the measured TSCS of two different stirrers at the University of Liverpool at 10 GHz to characterize the stirrer performance and to check if it is smaller than $A_s/4$.

The measurement setup is shown in Fig. 3. Two horn antennas were used (Rohde & Schwarz® HF 906 and SATIMO® SH 2000) and 10001 samples of *S*-parameters in the range of 9.8 GHz ~ 10.2 GHz were collected at each stirrer position. The vertical stirrer was rotated with 360 stirrer positions (1 degree/step); since we were measuring the TSCS of the vertical stirrer, the horizontal stirrer was fixed. After all the *S*-parameters were collected, a 10th-order elliptic band pass filter with 10 GHz center frequency and 200 MHz bandwidth was used to filter the *S*-parameters [7, 8]. The time domain impulse response can be obtained from the IFFT of the filtered *S*-parameters. The extraction procedure of τ_s is similar to the chamber decay time (τ_{RC}) extraction [7, 8]. τ_s can be extracted from the least-square fit of the logarithm of $C(t)$ in (7) [7, 8], as shown in Fig. 4; thus the measured TSCS can be obtained using $TSCS = V/(c_0\tau_s)$ [1]. $C(t)$ with different step degrees are also shown. It can be seen that, smaller step degrees (more sample number) can reduce the least-square fit error, and more available signals can be used for the least-square fit.

To obtain an averaged TSCS, we randomly changed the positions of antennas and the horizontal stirrer and repeated the measurement 10 times. The measured TSCS values of 10 random configurations are shown in Fig. 5(a). The limit of TSCS is also given. By removing one paddle we can have two different stirrers with the same stirring surface, shown in Fig. 5(b). Because the stirrer was close to the corner of the RC, the use of a cylinder as the equivalent boundary (stirring surface) would give an overestimated value. A better choice is shown in Fig. 3(b). Only surfaces that do not overlap with the walls of the RC contribute to the equivalent boundary. The dimensions are given in Fig. 3(b) and the maximum TSCS can be calculated as 10.6/4=2.65 m^2. As expected, all the measured TSCS values are smaller than the theoretical limit, and the ratio of $4TSCS/A_s$ can be used to characterize how close the stirrer is to a perfect diffuse wave scatterer. We use the average value to calculate the ratio. As can be seen, the removal of one paddle degrades the performance of the stirrer as expected. At 10 GHz, the one with 3 peddles is about 56% and the one with 2 peddles is about 44%, thus we can quantify the effectiveness of the stirrer.

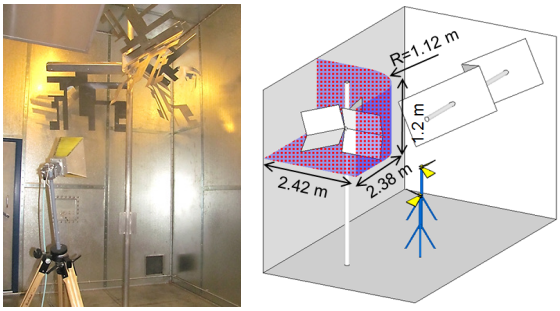

(a) (b)

Fig. 3. TSCS measurement setup in the RC, the size of the RC is 3.6 m (*W*) × 5.8 m (*L*) × 4 m (*H*). The equivalent boundary is shown in (b) with dots, the surface area is 10.6 m^2.

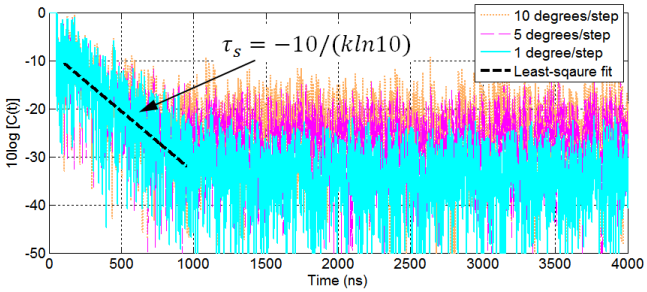

Fig. 4. Measured 10 log$[C(t)]$ with different step degrees, the *S*-parameters are filtered using an elliptical filter. $\tau_s = -10/(kln10)$, where k is the slope of the least-square fit line. Signals after 1000 ns are the noise floor and are not used for the least-square fit.

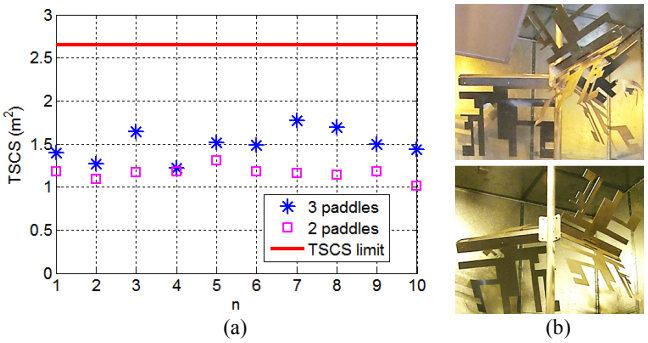

(a) (b)

Fig. 5. (a) Measured TSCS at 10 random RC configurations and the TSCS limit (solid line), (b) stirrers with 3 and 2 paddles.

IV. Discussion and Conclusions

In this letter, two dual scenarios in an RC have been analyzed

using a multipath model. Dual quantities are given in Table I. It has been found that there is a limit for the TSCS of an electrically large stirrer (a perfect diffuse wave scatterer). The value is a quarter of the stirring surface area. This means that optimized stirrer [10] can only approach but not exceed this limit. The ratio between the measured TSCS and the theoretical limit ($4TSCS/A_s$) can be used to characterize how well the stirrer is designed or how close it is to a perfect diffuse wave scatterer.

It should be noted that, although the derivation is for one stirrer, there is no difference for the case of an arbitrary number of stirrers, the derivation procedures are the same. Like the ACS, the TSCS also can be superimposed [1]. It can be found that, the measured averaged *S*-parameters in a perfect RC and perfect AC are the same, as shown in Fig. 6(a). The averaged multipath signals (from each stirrer position configuration) cancel each other. The averaged *S*-parameter is just the line-of-sight (LoS) path, which corresponds to a perfect anechoic chamber (AC) in Fig. 6(b). In this case, the measured $\langle S \rangle$ in an RC equals the measured *S*-parameter in AC (free space response). Thus the TSCS of a stirrer actually describes how close are the measured averaged *S*-parameter in an RC ($\langle S \rangle$) and the free space response in an AC ($S_{Freespace}$). This confirms the relationship between $\langle S \rangle$ and $S_{Freespace}$ in [11]. Especially when source stir is introduced [11-13], if we consider the rotating source as the origin of the frame of reference, rotating the source is actually rotating the whole RC, which has been proven to give a better performance [12, 13].

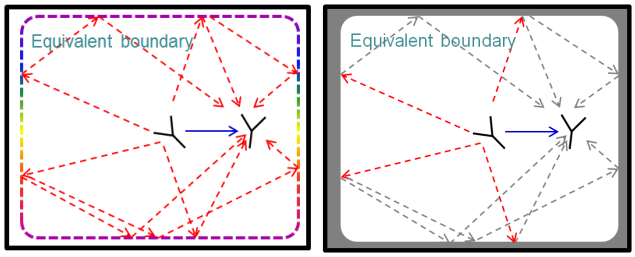

(a) (b)

Fig. 6. A perfect RC (a) and a perfect AC (b), waves with dashed lines in (b) are perfectly absorbed.

One can also use the TSCS of a stirrer to characterize how close the RC is to a perfect RC. Suppose the measured TSCS of a stirrer is $TSCS$, thus the surface area of the *equivalent* perfect diffuse wave scatterer is $4TSCS$. Suppose the stationary surface area (ground floor, walls, ceiling, *etc*) is A_{RC}, we can use $4TSCS/(4TSCS + A_{RC})$ to describe how large is the stirring surface area compared to the overall surface area (including the stirring surface) in the RC.

In this letter, we did not discuss the probability density functions (PDFs) of TSCS and ACS, since the Q (quality factor) can be considered as a random variable [14-16], which means τ_{RC}, τ_s and TSCS can also be treated as random variables. For the perfect absorber and the perfect diffuse wave scatterer, the PDFs of τ_{RC} (ACS) and τ_s (TSCS) can be the same, since they can have the same value for each measurement scenario (for each scenario, a dual scenario exists). Another interesting problem is that, in [1], a sphere was moved freely in the RC and the TSCS was found to be $2\pi a^2$ (electrically large), and a is the radius of the sphere, which is half of the surface area of the sphere. But in this letter, the maximum TSCS is $A_s/4$, the TSCS limit for a free moving object could be $A_s/2$, where A_s is the surface area of the minimum sphere that can cover the whole object. How to prove this could be the future work.

REFERENCES

[1] G. Lerosey and J. de Rosny, "Scattering cross section measurement in reverberation chamber," *IEEE Trans. EMC,* vol. 52, no. 2, pp.280-284, May. 2007.

[2] S. Lallechere, I. E. Baba, P. Bonnet and F. Paladian, "Total scattering cross section improvements from electromagnetic reverberation chambers modelling and stochastic formalism," in Proc. of the 5th European Conf. on Antennas and Propag. (EUCAP), pp. 81-85, Apr. 2011.

[3] I. E. Baba, S. Lallechere, P. Bonnet, J. Benoit and F. Paladian, "Computing total scattering cross section from 3-D reverberation chambers time modelling," in Proc. of Asia-Pacific Symp. on Electromagn. Compat. (APEMC), pp. 585-588, May 2012.

[4] P. Hallbjorner, U. Carlberg, K. Madsen and J. Anderson, "Extracting electrical material parameters of electrically large dielectric objects from reverberation chamber measurements of absorption cross section," *IEEE Trans. EMC*, vol. 47, no. 2, pp. 291-303, May 2005.

[5] E. Amador, C. Lemonie, P. Besnier and A. Laisne, "Reverberation chamber modeling based on image theory: investigation in the pulse regime," *IEEE Trans. EMC*, vol. 52, no. 4, pp. 778-789, Nov 2010.

[6] J. M. Ladbury and D. A. Hill, "Enhanced backscatter in a reverberation chamber: Inside every complex problem is a simple solution struggling to get out," in Proc. IEEE Int. Symp. Electromagn. Compat., pp. 1-5, Jul. 9-13, 2007.

[7] E. Genender, C. L. Holloway, K. A. Remley, J. M. Ladbury, G. Koepke and H. Garbe, "Simulating the multipath channel with a reverberation chamber: application to bit error rate measurements," *IEEE Trans. EMC,* vol. 52, no. 4, pp.766-777, Nov. 2010.

[8] C. L. Holloway, H. A. Shah, R. J. Pirkl, K. A. Remley, D. A. Hill and J. Ladbury, "Early time behavior in reverberation chambers and its effect on the relationships between coherence bandwidth, chamber decay time, RMS delay spread and the chamber buildup time," *IEEE Trans. EMC,* vol. 54, no. 4, pp.714-725, Aug. 2012.

[9] A. Gifuni, "On the measurement of the absorption cross section and material reflectivity in a reverberation chamber," *IEEE Trans. EMC*, vol.51, no.4, pp.1047-1050, Nov. 2009

[10] J. Clegg, A. C. Marvin, J. F. Dawson and S. J. Porter, "Optimization of stirrer designs in a reverberation chamber," *IEEE Trans. EMC,* vol. 47, no. 4, pp.824-832, Nov. 2005.

[11] P. –S. Kildal, C. Carlsson and J. Yang, "Measurement of free-space impedances of small antennas in reverberation chambers," *Microwave and Optical Technology Letters*, vol. 32, no. 2, pp. 112-115, Dec. 2001.

[12] Y. Huang and D. J. Edwards, "A novel reverberating chamber: source-stirred chamber," in Proc. of IEE 8th Int. Conf. on Electromagn. Compat., pp. 120-124, Sep. 1992.

[13] K. Rosengren, P. –S. Kildal, C. Carlsson and J. Carlsson, "Characterization of antennas for mobile and wireless terminals in reverberation chambers: improved accuracy by platform stirring," *Microwave and Optical Technology Letters*, vol. 39, no. 6, pp. 391-397, Sep. 2001.

[14] L. R. Arnaut, "Statistics of the quality factor of a rectangular reverberation chamber," *IEEE Trans. EMC*, vol. 45, no. 1, pp. 61–76, Feb. 2003.

[15] L. R. Arnaut and G. Gradoni, "Probability distribution of the quality factor of a mode-stirred reverberation chamber," *IEEE Trans. EMC*, vol. 55, no. 1, pp. 35–44, Feb. 2013.

[16] A. Gifuni, G. Ferrara, M. Migliaccio and A. Sorrentino, "Estimate of the probability density function of the quality factor of mode tuned, source stirred and mode stirred reverberation chambers," *IEEE Trans. EMC*, available online, DOI: 10.1109/TEMC.2015.2430525.